Research Paper

Holocene geomorphodynamics of a rural catchment in the Pergamon micro-region (eastern Mediterranean)

Xun Yang,[1] iD **Fabian Becker,**[1] iD **Moritz Nykamp,**[1] iD **Bernhard Ludwig,**[2] iD **Mehmet Doğan**[3] iD **and Brigitta Schütt**[1]

Abstract

The Pergamon micro-region (western Türkiye) has experienced several phases of increased geomorphodynamics during the Holocene. However, the role of local–regional human activities during a transformation between Hellenism and the Roman Imperial period and supra-regional climate fluctuations is still under discussion. Five sediment profiles from the alluvial fan of the rural Deliktaş catchment are analyzed and radiocarbon-dated to provide a sedimentological record covering the Holocene. Our results indicate seven phases of changing sediment dynamics. Five Holocene cycles of coarse- and fine-textured fan sediment deposition covered the paleochannel deposits of the Çaylak creek, and the floodplain sediments of the receiving Geyikli river which aggraded toward the piedmont during the Mid-Holocene. The landscape became stable on the Deliktaş fan and Geyikli floodplain at least ca. 4–3.4 cal ka BP as indicated by paleosols. These paleosols were again buried by fan sediments marking the first phase of accelerated geomorphodynamics during the Late Holocene. Both the local onset of human activities and the regional Mid-Holocene aridization with rapid climate changes play a role. The increased number of archeological sites and high human pressure on the environment during the Hellenistic–Roman transformation in the Deliktaş area and Pergamon micro-region were hypothesized to contribute to a phase of increased geomorphodynamic activity during the last 2.5 ka. This, however, is less apparent in our record. Our study emphasizes the importance of both, the climatic system and rural-urban cultural history, on landscape development, suggesting potential responses of locally diverse geomorphodynamics on regional-scale transformation in the eastern Mediterranean.

Keywords

alluvial fan, Bakırçay river, Holocene, human-environment interactions, Mediterranean area, sediment dynamics

Introduction

In the micro-region of the ancient city of Pergamon (Figure 1), known as a Hellenistic and Roman Imperial supra-regional administrative and cultural center (Knitter et al., 2013; Pirson, 2020), archeological remains reveal human occupation since ca. 11 ka BP (Aksan et al., 2022). After the Attalid kingdom bequeathed Pergamon to Rome in the second century BCE, the micro-region underwent a profound transformation characterized by population growth, doubling of the urban area, a vigorous public building program, a change of settlement structure, and demilitarization (Laabs and Knitter, 2021; Ludwig, 2023; Pirson, 2017, 2020; Wulf, 1994; Zimmermann, 2011). This transformation increased the intensity of human impacts on land use both in and around the city and its villages (Günther et al., 2021; Laabs and Knitter, 2021). Beyond, sediment archives from the micro-region indicate local-scale changing geomorphodynamics during the Middle and Late Holocene (Schneider et al., 2013, 2014, 2015; Seeliger et al., 2019; Yang et al., 2023), roughly corresponding to the fluctuations in hydroclimate, vegetation, and settlement activities in the micro-region and its neighboring areas (Becker et al., 2020). The intensified geomorphodynamics, in essence, correspond to soil erosion processes, as pointed out also for many areas in the eastern Mediterranean (Dusar et al., 2011; Roberts et al., 2019a; Walsh et al., 2019). However, the diversity of landforms (Yang et al., 2021), local

tectonics (Paradisopoulou et al., 2010), human activities, and regionally varying climatic changes caused intra-regional differences in landscape development (Dusar et al., 2011).

The eastern Mediterranean experienced a marked drying trend from around 4.6 ka BP (Finné et al., 2011) and several distinct rapid climate changes with locally varying intensity and timing (Bini et al., 2019; Weiss, 2016). The 4.2 ka BP drought event (between ca. 4.2 and 3.9 ka BP) (Bini et al., 2019; Roberts et al., 2011) and the later 3.2 ka BP drought event (two phases: 3.5–3.3 and 3.1–2.9 ka BP) (Hazell et al., 2022; Manning et al., 2020) are widely regarded as the most important rapid climate change events during the Mid- to Late Holocene (Bini et al., 2019; Di Rita et al., 2022). The influence of these events on the diverse landscapes in the eastern Mediterranean region (including the Pergamon micro-region) is not yet fully understood.

[1]Department of Earth Sciences, Institute of Geographical Sciences, Freie Universität Berlin, Germany
[2]Istanbul Department, Deutsches Archäologisches Institut (DAI), Türkiye
[3]Faculty of Letters, Department of Geography, Ege University, Türkiye

Corresponding author:
Xun Yang, Institute of Geographical Sciences, Department of Earth Sciences, Freie Universität Berlin, Malteserstraße. 74-100, Berlin 12249, Germany.
Email: xun.yang@fu-berlin.de

Figure 1. Topographical map with the locations of selected archeological sites (Ludwig, 2020b) and modern settlements in the Pergamon micro-region. The inset map indicates the location of this study in the Aegean coastal region of western Türkiye.

Located in the western Pergamon micro-region, the Karadağ mountain forms a peninsula, to the north, west, and south surrounded by the Aegean Sea. To the east, it verges on the floodplain of the lower Geyikli river, a major tributary of the Bakırçay river. The Deliktaş catchment drains the landside part of the Karadağ mountain (Figure 1). Widespread rills and gullies document severe soil erosion processes in the areas today covered by typical Mediterranean shrubland. Area-wide archeological surveys document that this area has been inhabited by humans at least since the Bronze Age; the number of settlement sites markedly increased during the Hellenistic–Roman Imperial period (Ludwig et al., 2022). Sequential subsurface stratigraphy correlative to the erosion processes in the transition zone of the Deliktaş fan and the Geyikli floodplain provides a suitable archive to document regional environmental variability of different spatial scales, which might be influenced by the drainage basin size and geology as well as their responses to climatic, tectonic, base-level changes (Van Dijk et al., 2012) and human influence (Coulthard et al., 2002; Dusar et al., 2011).

The overall objectives of this paper are to better understand (a) the complexity of local geomorphodynamics in the Pergamon micro-region, and (b) possible triggers of varying intensities of geomorphodynamic processes, that is, supra-regional climatic events and local to regional settlement activities. Comparing our findings with studies from the wider eastern Mediterranean allows us to decipher the effects of climate and humans as spatio-temporally varying forces on the Mediterranean landscape forming processes that are subject to debate for already more than 50 years (e.g. Dusar et al., 2011; Jouffroy-Bapicot et al., 2021; Vita-Finzi, 1969, and references therein). Beyond, this study will provide insights into how local landscapes respond to the (urban) transformation in the Mediterranean region.

## Study site

Natural setting

The Deliktaş catchment (ca. 15 km²) is located in the eastern Karadağ mountain (Figure 1) at the western tip of the graben-controlled Bakırçay plain (Karacik et al., 2007; Yang et al., 2021). The modern climate is typical Mediterranean subhumid, characterized

by prominent seasonality with dry and hot summers and mild and wet winters (Bakker et al., 2013; Peel et al., 2007). The close-by station in Dikili (Figure 1) recorded an annual precipitation of 711 mm and an annual temperature of 16.2°C (1981–2010) (Yang et al., 2021).

The Pergamon micro-region is located in one of the most rapidly extending regions on Earth (Özpolat et al., 2022), thus, being tectonically highly active, with at least nine earthquakes documented during the last two millennia (Emre et al., 2005; McHugh et al., 2006; Nalbant et al., 1998; Paradisopoulou et al., 2010; Schneider et al., 2014). A seismic landslide caused the abandonment of a rural settlement during the 20th century (Ludwig, 2020a). Pleistocene tectonics formed NW-trending normal faults within the Deliktaş catchment (Karacik et al., 2007). At present, the NE-trending Bakırçay (Bergama) graben is subsiding at a rate <1 mm yr⁻¹ (Seeliger et al., 2017). Situated in the Dikili-Çandarlı volcanic suite of the western Anatolian Miocene volcanism, the Deliktaş catchment is dominated by upper Miocene–Pliocene rhyolite domes of the Çandarlı group (Karacik et al., 2007) where lime-free brown soils developed (Danacioğlu and Tağil, 2017).

A field survey showed very strong geomorphodynamics all over the Deliktaş catchment (Figure 2). Slopes in the upper catchment are steep (average ca. 30°, calculated from TanDEM-X data with 12.5 m resolution) and dissected by intermittent drainage ways, mainly gullies (Becker et al., 2022a) (Figure 2b and c). Bare rocks crop out predominantly on the steep slopes in the headwater area where stony soils are ubiquitous (Figure 2c). The Çaylak creek flows eastwards into the Geyikli river, a major tributary of the Bakırçay river (Figure 1). At the transition from the Karadağ mountain to the Geyikli floodplain, the Çaylak creek deposits an alluvial fan (size: 1 km²; length: 1.6 km; slope: 1°; Figure 2).

Shrubs characterize the present-day vegetation cover of the Deliktaş area (Supplemental Figure S1, available online). Grasslands predominate in the northern part of the catchment; coniferous woodlands and olive groves prevail in its southern part (Figure 2c and d). From 7.6 to 3 ka BP natural deciduous oak forests prevailed around the nearby ancient harbor city of Elaia (Figure 1) (Shumilovskikh et al., 2016). A rather open landscape existed between 3.5 and 3.4 ka BP around the Kara Göl crater
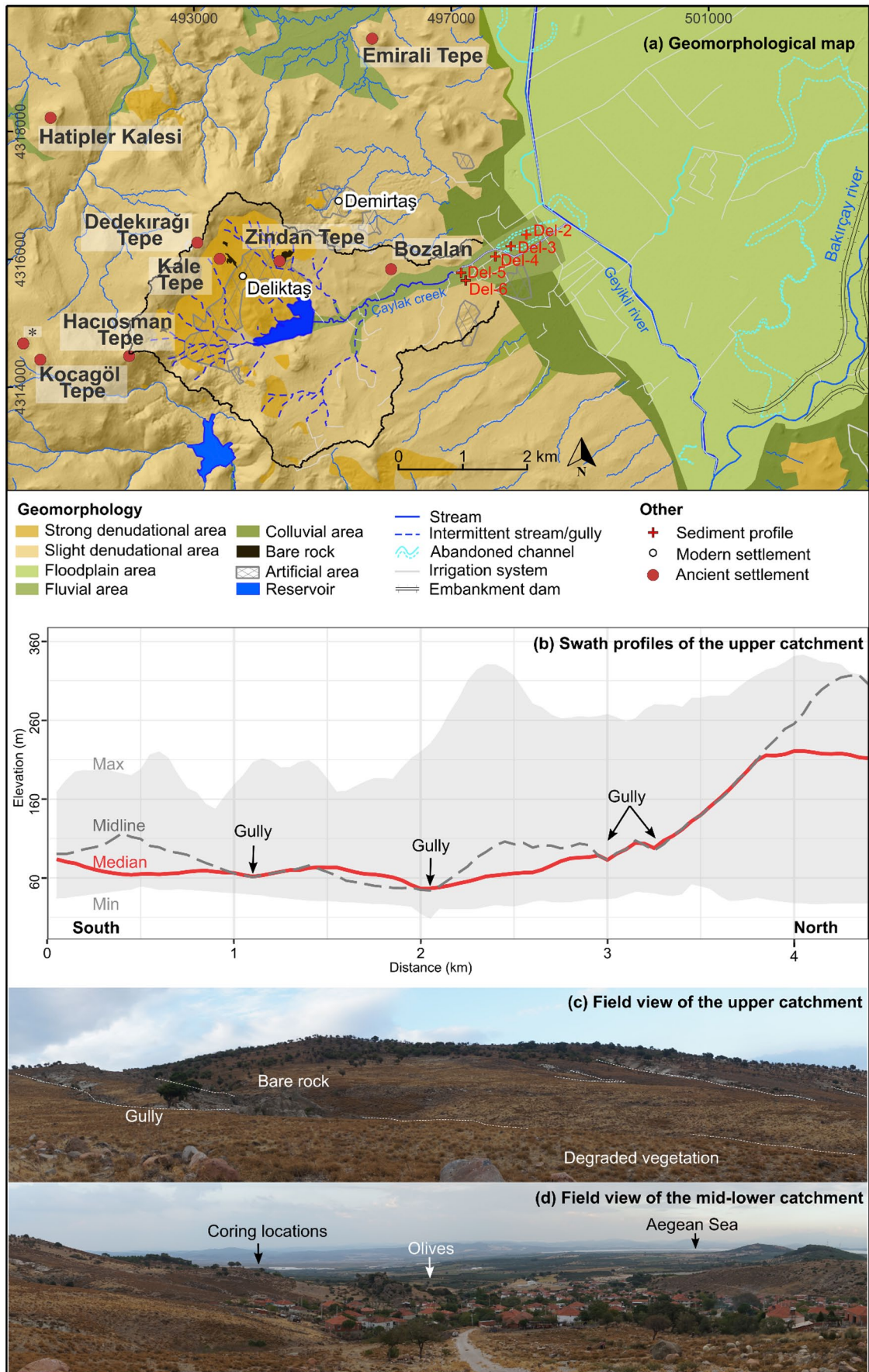
Figure 2. (a) Geomorphological map of the Deliktaş catchment complemented by the locations of the sediment profiles and ancient settlements (Ludwig et al., 2022). Note: *represents an unnamed archeological site. (b) Swath profiles of the upper Deliktaş catchment. (c) Field view of the upper catchment. (d) Field view of the mid–lower catchment. (Field pictures in c and d were taken on 10 Oct 2021 by the first author, which, together with figure b, were modified from Becker et al. (2022a).

Table 1. Metadata of sediment cores extracted from the Deliktaş alluvial fan (*n* = 5).

Sediment profile	Latitude (° N)	Longitude (° E)	Elevation (m a.s.l.)	Depth (cm b.s.)	Samples (*n*)	Geomorphological position
Del-2	38.99649	26.97883	6.0	500	33	Alluvial fan (distal area)
Del-3	38.99484	26.97604	7.1	700	46	Alluvial fan (middle area)
Del-4	38.99339	26.97326	9.3	800	39	Alluvial fan (middle area)
Del-5	38.99110	26.96710	12.5	444	28	Alluvial fan (proximal area)
Del-6	38.99000	26.96794	12.2	500	25	Alluvial fan (proximal area)

lake (Figure 1) (Shumilovskikh et al., 2022). Arboriculture (olive, pistachio, and walnut) extended during the Late Holocene, parallel to the spread of pastoral and tillage agriculture, likely reaching a maximum during 2.1–1.8 ka BP (Shumilovskikh et al., 2016, 2022). The spread of olives might also correspond with the contemporarily favorable climate conditions (Di Rita and Magri, 2009; Florenzano et al., 2017). In the past 1000 years, semi-natural forests (mainly pine) dominated whereas oak forests decreased (Shumilovskikh et al., 2016, 2022); olives are still cultivated. Overgrazing occurs in mountainous areas (Shumilovskikh et al., 2022).

Settlement history

The archeological survey in the Deliktaş catchment and its surroundings indicates settlement activities have started since the Bronze Age (two sites: Zindan Tepe and Hatipler Kalesi) (Figure 2; Supplemental Table S1, available online) (Ludwig et al., 2022). The number of archeological sites increased (*n* = 9) at the onset of the Classical period and remained high during the Hellenistic and Roman Imperial periods (ca. 500 BC–400 AD; Supplemental Table S1, available online) (Ludwig et al., 2022). Successively, only three sites were settled during the Late Antiquity, Byzantine, and Ottoman periods (Supplemental Table S1, available online).

Hilltop sites, for example, Zindan Tepe, were likely used as fortresses because they have an impressive view over the Bakırçay plain and to the cities of Pergamon, Elaia, and Pitane (Ludwig et al., 2022). Additionally, buildings in higher areas, for example, Dedekırağı Tepe and Hacıosman Tepe, are interpreted as watchtowers or tower houses as part of agricultural estates (Ludwig et al., 2022). The Deliktaş catchment is located adjacent to the major route network which connects the harbors of Pitane and Elaia with various sites in the Karadağ mountain (Fediuk et al., 2019; Laufer, 2015; Ludwig, 2020b; Figure 1).

Methods

Fieldwork

Five sediment profiles (thicknesses up to 8 m) were obtained along a transect from the proximal to distal area of the Deliktaş alluvial fan by vibracoring with open cores (5 cm diameter) in October 2021 (Figure 2; Table 1). The macroscopic sediment description included layer thickness, sediment color, depositional structure, texture and fabric, hydromorphic features, biological modification, and occurrence of artifacts (see also Yang et al., 2022). Sediment samples (*n* = 171) were taken according to stratigraphic layers; samples for radiocarbon dating (*n* = 12; Table 3) were also collected.

Laboratory work

Sediment analyses. Sediment samples were analyzed on six bulk parameters in the laboratory of the Bergama archeological excavation house to provide indicators for sediment origins, erosional and (post-) depositional processes (Buggle et al., 2011; Croudace and Rothwell, 2015; Ülgen et al., 2012), paleosol occurrence (Niwa et al., 2011; Nykamp et al., 2020) and human activity (Goldberg and Macphail, 2006). The aggregates of the air-dried samples were crushed. Coarse components (Ø ≥ 2 mm) were separated from fine fractions (Ø < 2 mm) and weighted to calculate the mass percentage of the coarse components. Electrical conductivity (EC) and pH values of the sediments were measured at least 2 times in a suspension of 5 g dried sediments in 12.5 mL distilled water by applying a PEZ9908 meter (resolution: 0.01 pH, 1 µS cm^{-1} EC). The pH classification refers to the USDA soil survey manual (Soil Science Division Staff, 2017) (Supplemental Table S2, available online). Mass-specific magnetic susceptibility of the sediments was determined by triplicate measurements of weighted samples at low frequency (X_{LF}, 10^{-8} m^3 kg^{-1}) in 12 cm^3 plastic pots with a Bartington magnetic susceptibility system (MS3 meter and MS2B dual frequency sensor) (Dearing, 1994; Dearing et al., 1996). Loss on ignition (LOI_{550}) as a proxy for organic matter content was measured by igniting 10 g sample materials at 550°C for 4 h in a muffle furnace after oven-drying the sediment (4 h at 105°C) (Dean, 1974; Heiri et al., 2001; Santisteban et al., 2004). Strong positive relationships between LOI_{550} and the total organic carbon content (Supplemental Figure S2, available online) of sediments from the western lower Bakırçay plain (Supplemental Figure S1, available online) indicate LOI_{550} in this region is capable to estimate organic matter content.

The elemental composition of samples from Del-2, Del-3, and Del-5 was analyzed using a portable energy-dispersive X-ray fluorescence spectrometer (p-ED-XRF; Thermo Fisher Scientific NITON XL3t-900 GOLDD+; analytical range: Mg to U) applying the "Mining Cu/Zn" mode with four filters (30 s measurement time each filter). Quality was controlled by measuring certified reference materials and acid-purified silica sand (Supplemental Table S3, available online). For elemental sediment characterization, we report the element ratios of Ca/Ti and K/Si.

Results of laboratory analyses are reported as median and median absolute deviation (MAD, in brackets) and categorized using the classifications in Supplemental Table S2, available online. Reported relationships between the variables were established based on Spearman's correlation coefficient and related tests (α = 0.05). The assumption of (bivariate) normality is tested by applying the Shapiro-Wilk test (*ggpubr v0.6.0* (Kassambara, 2023) and *corrplot v0.92* (Wei and Simko, 2021)) in R (R Core Team, 2022). Raw and processed data are provided in a published dataset at PANGAEA (Yang et al., 2023).

Radiocarbon dating. The sediment chronology is developed by radiocarbon dating (^{14}C) of charcoal or a mixture of charcoal and adhering sediments (the latter if %C of the macroscopically separable charcoal is < 1–2 mg) using accelerator mass spectrometry (AMS) at the TÜBİTAK National 1 MV AMS Laboratory (Doğan et al., 2021). Macroscopic plant remains and rootlets were removed before the samples were acid-washed (Brock et al., 2010; Fowler et al., 1986). The IntCal20 calibration curve (Reimer et al., 2020) and the *rcarbon* package (Crema and Bevan, 2021) were used to calibrate the radiocarbon ages in R (R Core Team, 2022). Confidence intervals of 95% are reported for the calibrated ages. The age-depth modeling of samples from profiles Del-2,

Table 2. The characteristics of sediment sub-facies in the Deliktaş catchment (cf. Yang et al., 2023).

Facies	Sub-facies		Description
Deliktaş alluvial fan sediments (B)	Ba	fine-textured alluvial fan sediments	characterized by clayey to silty sediments with occasionally distributed pebbles; often high in EC and LOI_{550} values; low X_{LF} and element ratio of K/Si
	sBa	recent or buried topsoil horizons developed on sub-facies Ba	clay/silt, a distinct increase in LOI_{550} values compared to sub-facies Ba
	Bb	coarse-textured alluvial fan sediments	more coarse components (mainly fine pebbly sand) with typically lower values of LOI_{550} and increased values of K/Si compared to sub-facies Ba
	Bc	channel deposits	layers of massive, clast-supported, subangular to subrounded fine–medium pebbles
Geyikli river sediments (C)	Cf	floodplain sediments of the Geyikli river	clayey to silty deposits; compared to sub-facies B, this sub-facies is slightly more alkaline and organic richer; enhanced Ca/Ti ratio and solutes (secondary carbonate precipitation); common Fe-Mn mottling (strongly influenced by the groundwater variation from the Geyikli floodplain)
	sCf	buried topsoil horizons developed on sub-facies Cf	silty clays, with increased LOI_{550} values, compared to sub-facies Cf
	Csh	extreme flood events of the Geyikli river	thin layers (ca. 10 cm thick) of (fine pebbly) coarse sand intercalated within sub-facies Cf

Del-3, and Del-6 are calculated based on the *clam* R-package (v2.5.0) (Blaauw, 2010).

Sediment facies

Sediments extracted along the transect on the Deliktaş fan are categorized into seven sub-facies based on their macroscopical/lithological and (bulk-)chemical characteristics. These sub-facies are summarized into facies B, alluvial fan facies, and facies C, floodplain facies (Table 2). The classification resembles the facies described in Tekkedere alluvial fan (Yang et al., 2023), following the conventional sedimentological terminology of alluvial fan (Blair and McPherson, 1994, 2009; Moscariello, 2018) and floodplain deposits (Miall, 2006, 2014).

Facies B: Deliktaş alluvial fan sediments

The Deliktaş alluvial fan facies B contains four sub-facies (Table 2). Clayey to silty deposits with occasionally distributed pebbles are classified as fine-textured alluvial fan sediments (sub-facies Ba) which show generally high EC and LOI_{550} values, low X_{LF} values, and low element K/Si ratios. Repeatedly sub-facies Ba is topped by a layer with distinctly increased LOI_{550} values indicating recent or buried top-soil horizons (sub-facies sBa). Sub-facies Bb is composed of fine-pebbly sands with typically, compared to sub-facies Ba, low LOI_{550} values and increased K/Si ratio, corresponding to coarse-textured alluvial fan sediments. Massive, subangular to subrounded fine–medium pebbles represent channel deposits (sub-facies Bc) (Miall, 2006).

Facies C: Geyikli river sediments

Facies C, the Geyikli river sediments, includes three sub-facies (Table 2). Dark brown clayey to silty deposits, slightly alkaline and rich in organic matter are classified as sub-facies Cf, corresponding to floodplain sediments of the Geyikli river. Thin layers (ca. 10 cm thick) of coarse sand to fine pebble (sub-facies Csh) intercalate with these floodplain sediments and correspond to stronger flood events compared to sub-facies Cf (Miall, 2006). Silty clays with high LOI_{550} values overlying sub-facies Cf represent buried top-soil horizons developed on the floodplain sediments (sub-facies sCf).

Sediment profiles

The sediment profiles show alternating layers of alluvial fan deposits, which are generally coarser in the profiles extracted from the proximal fan and finer downslope. At the distal part, fan deposits interfinger with floodplain deposits of the Geyikli river. Sediment core Del-3 serves as a key profile and is presented in detail (Figure 3). The other sediment profiles are presented in overview and compared with the key profile Del-3; detailed documentation is provided in the Supplemental Materials, available online. Radiocarbon datings document that fan deposition started at least in the Early Holocene and continued during the entire Holocene, and the Geyikli floodplain deposits occurred during the Middle Holocene (Figure 3; Table 3).

Key profile Del-3

Key profile Del-3 was taken from the middle part of the Deliktaş fan and is 700 cm thick. It is subdivided into 9 lithostratigraphic units (Figure 3). A pebble-dominated unit at the bottom (unit 1; channel deposits, sub-facies Bc) is overlain by repetitions of sandy (units 2, 4, 6, and 8; coarse-textured alluvial fan deposits, sub-facies Bb) and silty-clayey (units 3, 5, 7, and 9; fine-textured alluvial fan deposits, sub-facies Ba) sediments. A radiocarbon sample from unit 2 dates into the Early Holocene (ca. 8.7 cal ka BP at 569 cm b.s.; Table 3). At approximately 1 m depth below the surface (unit 7, 117 cm b.s.) fan deposits are of Late Holocene age dating to ca. 3.6 cal ka BP. Accordingly, in the approximately 4.5 ka between the Early Holocene and the beginning of the Late Holocene about 4 m of sediments were accumulated. The charcoal-based radiocarbon age extracted from unit 5 (285 cm b.s.) with an age of 5.4 ka BP is in line with the aggradation rates.

In total, 46 samples were extracted from Del-3. Graphs displaying the amount of coarse fraction (particles $\varnothing \geqslant 2$ mm; 0–61 mass%) and K/Si ratios run highly parallel ($p < 0.001$, rho = 0.64), and show inverse trends to the graphs of EC ($\varnothing \geqslant 2$ mm and EC: $p = 0.05$, rho = -0.29; K/Si and EC: $p < 0.001$, rho = -0.58) and LOI_{550} values ($\varnothing \geqslant 2$ mm and LOI_{550}: $p < 0.001$, rho = -0.71; K/Si and LOI_{550}: $p < 0.001$, rho = -0.73; Figure 3). Values of pH remain roughly constant at 7.8 below 353 cm b.s. (units 1–4), slightly increase to 8.5 at 60 cm b.s., and drop rapidly to 6.9 near the surface. X_{LF} values decrease slightly oscillating from 71 10^{-8} m^3 kg^{-1} (class 3) in unit 1 to 36 10^{-8} m^3 kg^{-1} (class 2) in unit 4 and remain constantly low at ca. 23 10^{-8} m^3 kg^{-1} (class 1) in units 5–9. The element ratio of Ca/Ti remains relatively constant with values between 3 and 5. Altogether, sediments are poor in carbonates; only few carbonate precipitations occur around 280 cm b.s.

Unit 1 (700–647 cm b.s., $n = 3$) is characterized by matrix-supported, poorly sorted, coarse sand and (sub)rounded fine–coarse pebbles. Water-saturated sediments below 660 cm b.s. indicate the level of the current groundwater table. This unit has a
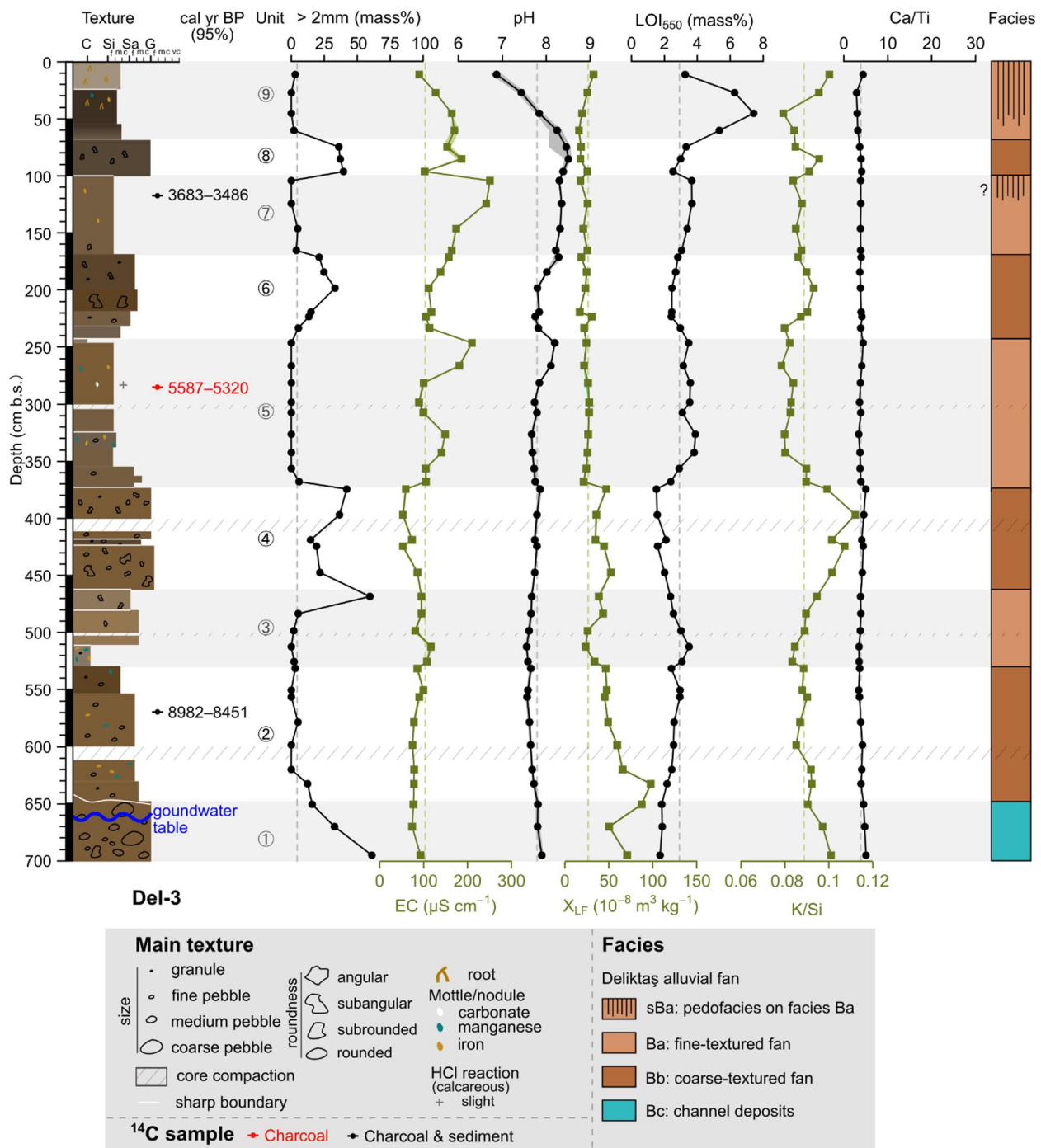
Figure 3. The lithostratigraphy, radiocarbon datings, sediment bulk characters, and sediment facies of profile Del-3. (1) colors of the sediment texture column represent the color observed in the field; (2) shaded bands separate different units; (3) the vertical dashed lines of each sedimentary analysis represent the median values of the whole profile.

sharp boundary to overlying unit 2. Three sediment samples show a distinctively decreasing content of coarse components (from 61 to 16 mass%) with decreasing depth; in parallel, K/Si ratios constantly decrease. This pebbly unit is interpreted as channel sediments (sub-facies Bc).

Unit 2 (647–528 cm b.s., $n = 7$) contains dark yellowish brown (10 YR 4/4) fine–medium sand with few fine pebbles and Fe-Mn mottles. It gradually transits to unit 3. The mixed charcoal/sediment sample at 569 cm b.s. dates to 8982–8451 cal yr BP (Table 3). EC values remain distinctly low (around 78 μS cm^{-1}) in units 1–2. X_{LF} values reach the highest number of Del-3 at the bottom of unit 2 (98 10^{-8} m^3 kg^{-1}) and decrease gradually to the unit top (46 10^{-8} m^3 kg^{-1}). LOI$_{550}$ values constantly increase from 1.7 mass% at the bottom of unit 1–3 mass% at the top of unit 2. K/Si

ratios slightly decrease from 0.092 to 0.088 with decreasing depth. This sandy unit corresponds to the coarse-textured alluvial fan facies (sub-facies Bb).

Unit 3 (528–461 cm b.s., $n = 5$) is composed of yellowish brown (10 YR 5/4) fine to medium sand in the upper layers and Fe-Mn mottled silty clay in the lower layers; few subrounded fine–medium pebbles occur. The boundary to overlying unit 4 is sharply marked by an increased content of coarse clasts (Ø ⩾2 mm). EC (96 (10) μS cm^{-1}) and LOI$_{550}$ (2.95 (0.4) mass%) in unit 3 are slightly higher than those in underlying units, however, predominantly marked by peaking values at ca. 510 cm b.s. (Figure 3). In contrast, K/Si ratios continuously increase from the unit bottom (0.083) to the top, reaching the maximum value in overlying unit 4 (0.11 at 400 cm b.s.). X_{LF} values slightly vary but

Table 3. The AMS-^{14}C dating samples from the Deliktaş alluvial fan ($n = 12$), pre-treatment procedure, sediment sub-facies of the sample location, and their dating results and calibration (calibration curve: IntCal20 (Reimer et al., 2020)). Dated material: C/S refers to mixed materials (charcoal and adhering sediment); sub-facies characteristics are in Table 2.

Sediment profiles	Depth cm b.s. (Unit ID)	Lab. ID (TÜBİTAK*)	Dated material	Sub-facies	^{14}C $\pm$ σ	cal BP Median	95% probability	CE/BCE (95%)
Del-2	226 (⑤)	2202	C/S	sCf	3215 ± 26	3423	3478–3378	1529–1429 BCE
	322 (③)	2203	charcoal	Cf	4092 ± 40	4605	4817–4444	2868–2495 BCE
	459 (①)	2204	C/S	Cf	6152 ± 30	7056	7157–6956	5208–5007 BCE
Del-3	117 (⑦)	2205	C/S	Ba	3348 ± 27	3570	3683–3486	1734–1537 BCE
	285 (⑤)	2206	charcoal	Ba	4735 ± 73	5466	5587–5320	3638–3371 BCE
	569 (②)	2207	C/S	Bb	7843 ± 76	8655	8982–8451	7033–6502 BCE
Del-4	85 (⑤)	2208	C/S	Ba	2227 ± 31	2227	2336–2148	387–199 BCE
Del-5	77 (⑤)	2209	C/S	Ba	3666 ± 97	4001	4290–3699	2341–1750 BCE
	230 (③)	2210	C/S	sBa	3541 ± 37	3828	3960–3699	2011–1750 BCE
Del-6	77 (④)	2211	charcoal	Ba	421 ± 21	495	515–343	1435–1607 CE
	166 (③)	2212	charcoal	sBa	1290 ± 22	1225	1283–1177	667–773 CE
	333 (②)	2213	charcoal	Bb	1598 ± 23	1470	1529–1411	421–539 CE

remain in low ranges (39 (7) 10^{-8} m^3 kg^{-1}). This clayey–fine sandy unit is a fine-textured alluvial fan facies (sub-facies Ba).

Unit 4 (461–371 cm b.s., $n = 5$) contains dark yellowish brown (10 YR 4/4) fine to coarse sand with subangular–subrounded fine pebbles. To the top, the unit gradually merges into unit 5 without a sharp boundary. Unit 4 is characterized by varying contents of coarse clasts (Ø ≥ 2 mm) on an altogether high level with approximately 15–42 mass%. EC values remain stable at a low level (60 (7) μS cm^{-1}). LOI$_{550}$ values oscillate around 1.6 mass% and reach the lowest content of 1.5 mass% at 374 cm b.s. K/Si ratios peak at 400 cm b.s. (K/Si = 0.11); in the underlying samples K/Si ratios constantly increase until peaking and then to the top constantly decrease. X$_{LF}$ values vary around 45 (7) 10^{-8} m^3 kg^{-1} without a distinct trend. Unit 4 is interpreted as coarse-textured fan deposits (sub-facies Bb).

Unit 5 (371–241 cm b.s., $n = 9$) is composed of dark yellowish brown (10 YR 4/4) clayey silt with few Fe-Mn mottles. Few fine carbonate nodules occur in the upper part. The boundary to overlying unit 6 is sharp. The charcoal sample from 285 cm b.s. dates to 5587–5320 cal yr BP. Values of LOI$_{550}$ slightly vary around 3.48 (0.3) mass% (class 3) and are higher than those in underlying units 1–4 (2.4 (0.5) mass%, $n = 20$). EC values distinctly increase from units 1 to 4 (80 (8) μS cm^{-1}, $n = 20$) to unit 5 with a median value of 106 (16) μS cm^{-1}, peaking at the boundary to overlying unit 6 (210 μS cm^{-1} at 246 cm b.s.). X$_{LF}$ values remain at an altogether low level around 26 (2) 10^{-8} m^3 kg^{-1} (class 1). Also, K/Si ratios remain stable around 0.08. This silty unit corresponds to fine-textured fan deposits (sub-facies Ba).

Unit 6 (241–168 cm b.s., $n = 6$) consists of dark brown (10 YR 3/3) fine to medium sand with few subangular–subrounded pebbles. It has a gradual boundary to overlying unit 7. Similar to unit 4, this unit shows relatively high contents of coarse clasts (Ø ≥ 2 mm; 18 (6) mass%). K/Si ratios (median = 0.09) are slightly higher than those in underlying unit 5. The values of pH (7.82) and EC (105 μS cm^{-1}) vary on a relatively low level; while above 200 cm b.s., pH values slightly increase to 8.3 and EC values increase to 158 μS cm^{-1} at the unit top. Values of LOI$_{550}$ remain constantly low without distinct variations (2.57 (0.1) mass%). This sandy unit represents coarse-textured fan deposits (sub-facies Bb).

Unit 7 (168–100 cm b.s., $n = 4$) is composed of brown (10 YR 4/3), Fe-mottled clayey silt. It sharply borders overlying unit 8. The mixed charcoal/sediment sample from 117 cm b.s. dates to 3683 to 3486 cal yr BP. EC values continuously increase from bottom to top and peak at the boundary to overlying unit 8 (251 μS cm^{-1}, 105 cm b.s.). Sediments are moderately alkaline

(pH = 8.31(0)). This silty unit corresponds to fine-textured fan deposits (sub-facies Ba). The slight increase of LOI$_{550}$ from 3.1 mass% at the unit base to 3.7 mass% at the unit top may imply an initial soil formation though other soil features are not apparent (Figure 3).

Unit 8 (100–68 cm b.s., $n = 3$) is composed of brown (10 YR 3/2) coarse sand with fine subangular to subrounded pebbles. It has a gradual boundary with overlying unit 9. Bulk sediment characteristics correspond to those in coarse-textured units (units 2, 4, and 6), dominated by high contents of coarse clasts, low EC and LOI$_{550}$ values, and peaking K/Si ratios. Correspondingly, this unit represents coarse-textured fan deposits (sub-facies Bb).

Unit 9 (68–0 cm b.s., $n = 4$) contains fine sandy silt with color changing from very dark brown (10 YR 2/2) at the bottom to light brownish gray (10 YR 6/2) at the top. The occurrence of roots increases to the surface. The values of pH constantly decrease from 8.3 at 60 cm b.s. to 6.9 at 11 cm b.s. The graph of EC values runs parallel to the graph of pH values, reaching low values around 90 μS cm^{-1} close to the surface (Figure 3). LOI$_{550}$ peaks with 7.4 mass% at 45 cm b.s. The graph of the K/Si ratio runs inversely to that of LOI$_{550}$, reaching minimum values of 0.08 at 50 cm b.s. This silty unit corresponds to fine-textured fan deposits (sub-facies Ba), modified by soil formation (sub-facies sBa).

Other Deliktaş fan sediment profiles

Sediment profile **Del-2** was extracted from the distal part of the Deliktaş alluvial fan (Figure 2). This 500-cm-thick profile shows 7 lithostratigraphic units (Figure 4A and Supplemental Figure S3, available online). Dark brown clayey to silty sediments dominate the bottom strata with occasional pebbles (units 1–5, below ca. 210 cm b.s.). LOI$_{550}$ values in units 1–5 ($n = 24$) average 3.3 (0.6) mass% and peak at 345 cm b.s. with 5.4 mass% (unit 3) and at 222 cm b.s. with 5.1 mass% (unit 5). K/Si ratios slightly vary (0.078 (0.004)) in these units, while Ca/Ti ratios show three times higher values in units 3 and 4 (12.5 (1), $n = 9$, 345–262 cm b.s.) than those in other units (4.162 (0.68), $n = 24$). Secondary carbonate concretions and Fe–Mn mottles are abundant in units 3–4. Due to the overall sediment characteristics of units 1–5, these deposits are assigned as floodplain deposits of the Geyikli river (sub-facies Cf). The transition between the floodplain and overlying alluvial fan deposits, corresponding to unit 5, shows the dark brown color of the sediments with high LOI$_{550}$ values (4.35 (0.2) mass%, class 3, $n = 4$) and in parallel relatively low pH (7.93 (0), $n = 4$) and locally peaking EC value and low K/Si values. Correspondingly, unit 5 is interpreted as a fossil soil developed on the
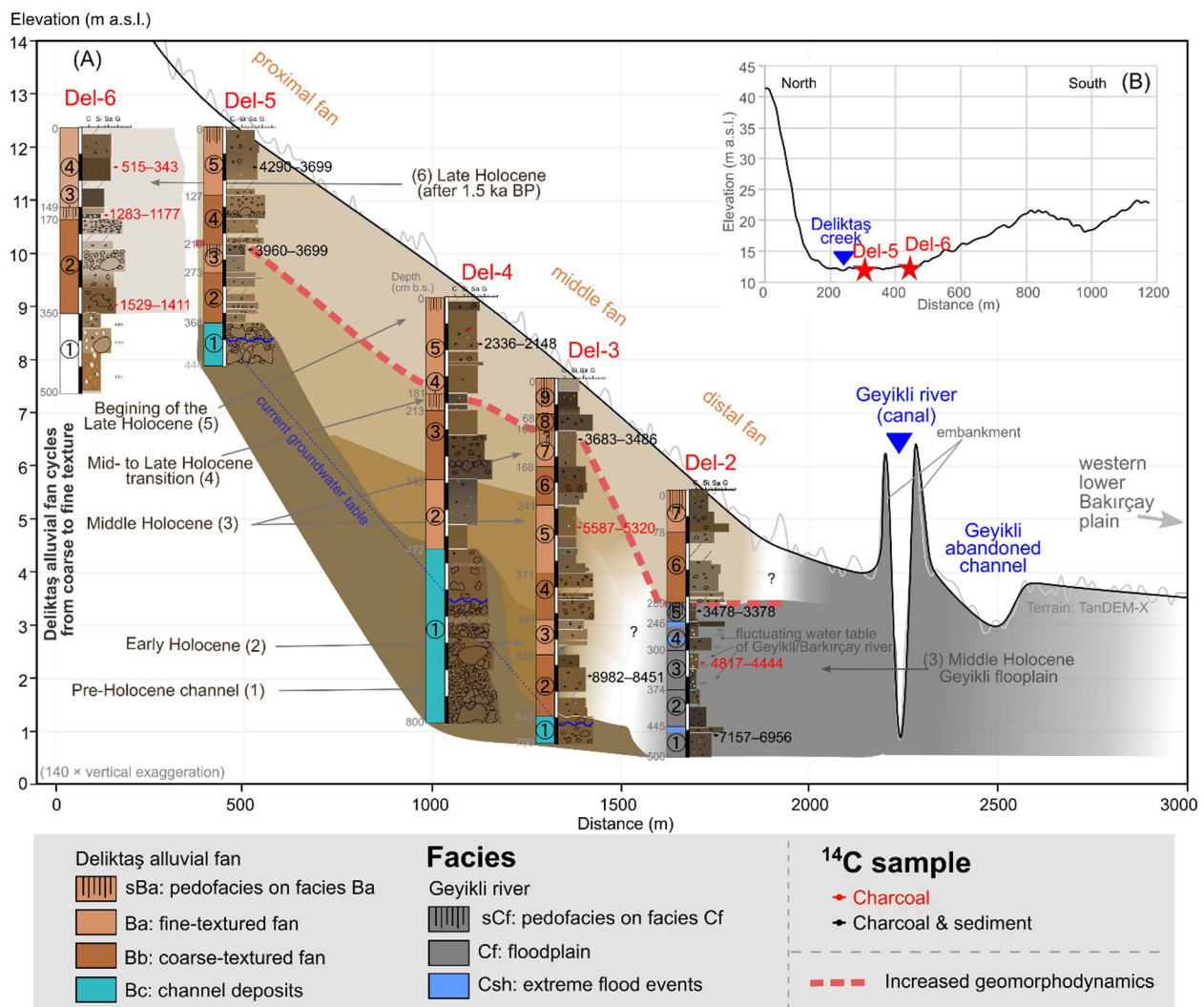
Figure 4. (A) The sediment profiles at a longitudinal transect on the Deliktaş alluvial fan (140 × vertical exaggerations). Note the background colors of brown and gray show the correlations of sediment facies among different profiles. (B) The location of the profiles Del-5 and Del-6 at a cross section on the Deliktaş alluvial fan (10 × vertical exaggerations).

floodplain deposits (sub-facies sCf). Fine pebbly sand layers in units 1, 4, and 5 point to high flood events (sub-facies Csh). In the uppermost layers of Del-2 (units 6–7, above 200 cm b.s.) grain sizes increase, showing dominating sand (unit 6, 208–78 cm b.s., sub-facies Bb) and silt (unit 7, 78–0 cm b.s., sub-facies Ba) components. LOI_{550} values in the two units remain low with poor variations (2.5 (0.3) mass%, $n=9$). Three radiocarbon datings from units 1 to 5 indicate that the Geyikli floodplain sediments were deposited from the Middle Holocene (7157–6956 cal ka BP, 450 cm b.s., unit 1) to the beginning of Late Holocene (3478–3378 cal ka BP, 226 cm b.s., unit 5) (Table 3). Accordingly, the overlying units 6 and 7, that is, the Deliktaş fan deposits, were accumulated during the Late Holocene.

Sediment profile **Del-4** was extracted from the middle part of the alluvial fan (Figure 2). This profile is 800 cm thick and divided into 5 lithostratigraphic units (Figure 4A and Supplemental Figure S4, available online). The stratigraphy and bulk-chemical characteristics of the sediments are comparable to those described for the key profile Del-3. The sediments with clast-supported fabric at the profile bottom (unit 1, 800–472 cm b.s.) refer to channel deposits (sub-facies Bc). They are overlain by fine-textured alluvial fan sediments (sandy to silty, unit 2, 472–343 cm b.s. and unit 5, 181–0 cm b.s.) corresponding to sub-facies Ba and coarse-textured alluvial fan sediments (pebbly to sandy, unit 3, 343–213 cm b.s.) corresponding to sub-facies Bb. Unit 4 (213–181 cm b.s.) is characterized by dark brown clayey silt with slightly increased values in EC, pH, and LOI_{550}, most likely documenting a fossil

soil (sub-facies sBa). A non-diagnostic ceramic fragment occurred at 60 cm b.s. The only radiocarbon sample taken from Del-4 (charcoal/sediment mixture from 85 cm b.s.) dates to 2336–2148 cal yr BP (Table 3).

Sediment profile **Del-5** is 444 cm thick and was extracted from the proximal fan (Figure 2). Del-5 shows five lithostratigraphic units (Figure 4A and Supplemental Figure S5, available online). Similar to the key profile Del-3, the basal sediments with a clast-supported fabric point to pebbly channel deposits of sub-facies Bc (unit 1, 444–368 cm b.s.) that are covered by alternating units of coarse-textured alluvial fan sediments of sub-facies Bb (unit 2, 368–273 cm b.s. and unit 4, 219–127 cm b.s.) and fine-textured alluvial fan sediments of sub-facies Ba (unit 3, 273–219 cm b.s. and unit 5, 127–0 cm b.s.). Brown clayey silts at the top of unit 3 (242–219 cm b.s., $n=2$) show relatively high LOI_{550} values (2.9 mass%) and relatively low pH values (7.88), suggesting a fossil soil. The mixed charcoal/sediment material extracted from this fossil soil dates to 3960–3699 cal yr BP (230 cm b.s.; Table 3). However, a radiocarbon age of the charcoal/sediment material from 77 cm b.s. (unit 5) dates to 4290–3699 cal yr BP (Table 3), indicating an age inversion.

Sediment profile **Del-6** was extracted from the transitional area of the proximal part of the alluvial fan and the toe of the adjoining hillslope (Figures 2 and 4B). Del-6 has a total thickness of 500 cm and is subdivided into four lithostratigraphic units (Figure 4A and Supplemental Figure S6, available online). The basal layers (unit 1, 500–350 cm b.s.) are composed of soft clayey silt to the bottom

passing over into weathered bedrock. Along the sediment profile of Del-6 (pH: 8.06 (0.3); EC: 137 (56) µS cm^{-1}; X_{LF}: 35 (11) 10^{-8} m^3 kg^{-1}), samples from the in-situ weathered bedrock ($n=10$) show the highest pH (8.56 (0.1)) and EC values (208 (26) µS cm^{-1}) and the lowest X_{LF} values (22 (4) 10^{-8} m^3 kg^{-1}). This material is overlain by pebbly sand corresponding to coarse-textured alluvial fan deposits (sub-facies Bb, unit 2, 350–170 cm b.s.), which merges into a fossil soil (sub-facies sBa, unit 3, 170–149 cm b.s.). The structure in unit 3 is crumbly and porous; X_{LF} (74 (49) 10^{-8} m^3 kg^{-1}, $n=2$) and LOI$_{550}$ values (5.42 (0.1) mass%, $n=2$) show a sharp increase. The light yellowish-brown color at the top of unit 3 (160–149 cm b.s.) might indicate burning at the soil surface (cf. Terefe et al., 2008). Unit 4 consists of sandy silt corresponding to fine-textured alluvial fan deposits (sub-facies Ba, 149–0 cm b.s.). Along the sediment profile of Del-6, three charcoal samples date the alluvial fan sediments of Del-6 from 1529–1411 cal yr BP (333 cm b.s.) to 515–343 cal yr BP (77 cm b.s.; Table 3).

Holocene geomorphodynamics

The analyses of sediment profiles from the area of the Deliktaş alluvial fan indicate rapidly changing depositional processes during the Holocene (Table 4). Based on the facies classification, seven major geomorphodynamic phases can be deduced (Figure 4A).

Pre- to Early Holocene (phases 1–2)

The gravel deposits (sub-facies Bc) form the base of profiles Del-3, Del-4, and Del-5 corresponding to channel sediments accumulated by the Çaylak creek (phase 1; Table 4) (cf. Brown, 1997). Locally, channel infills reach up to 3 m thickness (Del-4). The alluvial fan was dominated by channelized flows during this phase (cf. Parker, 1999). At key-profile Del-3, sediments overlying the channel infills date into the Early Holocene (9.0–8.4 cal ka BP, unit 2, 569 cm b.s.; Figure 4A; Table 3), indicating that the channel infills were possibly deposited in the Late Pleistocene. This observation is in line with various reports across the Mediterranean region describing such active channel erosion and subsequent channel infills for the Late Pleistocene (Bintliff, 2002; Vita-Finzi, 1969).

Alluvial fan deposits with changing textures covered these pre-Holocene channel infills (Figure 4A). The first cycle of coarse-textured alluvial fan sediments (sub-facies Bb) and fine-textured alluvial fan sediments (sub-facies Ba) occurs at the middle–distal part of the alluvial fan (Del-3, units 2–3) with a radiocarbon age dating to the Early Holocene (phase 2; Table 4). The change from sediment sub-facies Bb (coarse texture) to sub-facies Ba (fine texture) represents the conditions of surface runoff changing from high energy to low energy (Blair and McPherson, 2009). This might indicate (a) the shifting location of the Çaylak creek channel on the fan causing alternating depositional environments (cf. Blair and McPherson, 1994, 2009) or (b) alternating intensity of flood events (predominantly triggered by varying climate) (Bull, 1991; Dorn, 1994). The hydro-climatic conditions in the eastern Mediterranean region during the Holocene suggest temporal oscillations between wet and dry periods (Eastwood et al., 2007; Finné et al., 2019; Ocakoğlu et al., 2022), directly affecting run-off dynamics (Dorn, 1994) and hereby processes of erosion and deposition (Dusar et al., 2011). The influence of tectonic activity cannot be proven for the Deliktaş catchment where no major Pleistocene faults are known; however, the catchment is located at a horst structure in a tectonically active area, thus surrounded by fault lines (Karacik et al., 2007).

Middle Holocene (phase 3)

Another cycle of coarse- and fine-textured alluvial fan deposits is observed at the key profile Del-3 (units 4–5) and Del-4 (unit 2),

both located at the middle fan (Figure 4A). The radiocarbon datings from the upper part of the cycle (Del-3, unit 5, 285 cm b.s.) indicate that the sediments were deposited at least until 5.3 cal ka BP, thus during the Middle Holocene. Later, also during the Middle Holocene, the fine-textured fan deposits at the top of this cycle were covered by an analogous cycle of fan sediments, which extends from the proximal fan (Del-5, units 2–3) to the middle fan (Del-3, units 6–7; Del-4, units 3–4) (Figure 4A). The two cycles together form the third phase (Table 4). These findings indicate (a) a continuous growth of the spatial extent of the Deliktaş alluvial fan since the Early Holocene due to the topography of the channel base, allowing the space for fan growth (Figure 4A) or (b) remobilization processes from the proximal toward the distal area of the fan (cf. Van Dijk et al., 2012). Fan growth remained consistent until the beginning of the Late Holocene in the first assumption as indicated by the constant aggradation rate at Del-3 between ca. 9 and 3.5 cal ka BP (89 cm ka^{-1}; Figure 5). Alternatively, repeated re-deposition processes in a fan environment with shifting channels under a climate characterized by strong seasonality with torrential run-off have to be considered, particularly in its proximal area where the incision and backfilling processes are the most prominent during the experiments by Van Dijk et al. (2012).

Contemporarily (phase 3), the floodplain of the Geyikli river aggraded and prograded to the foreland of the Deliktaş fan, that is, the footslopes of the Karadağ mountain (Del-2; Table 4). This floodplain accumulation (sub-facies Cf) lasted from ca. 7 to 3.4 cal ka BP (ages from Del-2, unit 1, 459 cm b.s., and unit 5, 226 cm b.s.; Table 3), which was occasionally interrupted by stronger Geyikli flood events (sub-facies Csh; Figure 4A) and post-sedimentary influenced by carbonate-rich groundwater tables indicated by Fe-Mn mottles and increased Ca/Ti values in units 3 and 4 (Figure 4A and Supplemental Figure S3, available online) (cf. Goldberg and Macphail, 2006). The interfingering of Deliktaş fan and Geyikli floodplain deposits cannot be proven for this period.

Mid- to Late Holocene transition (phase 4)

At the top of the second cycle during the third phase, the fine-textured alluvial fan deposits are influenced by pedogenic processes (sub-facies sBa; Del-4, unit 4; Del-5, unit 3) indicating stable geomorphodynamic conditions without striking erosion and deposition processes (phase 4; Table 4). Pedofacies sBa in Del-5 dates to 3960–3699 cal yr BP (unit 3, 230 cm b.s.), whereas in Del-3 it was slightly younger with an age of 3683–3486 cal yr BP (unit 7, 117 cm b.s.; Table 3). On the Geyikli floodplain, a layer of paleosol (sub-facies sCf) at Del-2 dates again to a slightly younger age of 3478–3378 cal yr BP (unit 5, 226 cm b.s.; Table 3). These fan–floodplain soil processes indicate locally (at least at the coring locations) reduced landscape dynamics at the transition from the Middle to Late Holocene (at least during ca. 4–3.4 cal ka BP), a long-lasting period that allowed the development of 30–40 cm thick solum (Figure 4A).

Mid-Holocene low geomorphodynamics were also observed at a regional scale, for example, in the nearby Tekkedere catchment around 5–4 cal ka BP (Yang et al., 2023) and the western lower Bakırçay plain (Pergamon micro-region) around 4.3–4 ka BP (Becker et al., 2020). Simultaneously, low accumulation rates are reported during ca. 5.8–3.7 ka BP at Lake Gölhisar, SW Türkiye (Eastwood et al., 2007) and during ca. 4.3–4 ka BP in Pasinler Basin, eastern Türkiye (Collins et al., 2005). Although the phases of low erosion/deposition rate in these studies occurred earlier than that in the Deliktaş catchment, they all potentially correspond to the periods of supra-regionally (eastern Mediterranean) low climatic erosion sensitivity with a reduction in Mid-Holocene precipitation (Finné et al., 2011; Roberts et al., 2011). The contemporary limited human activities might also have

Table 4. Summary of the (pre-)Holocene sediment characteristics (a), depositional processes (b), and landscape and settlement dynamics (c) in the Deliktaş area.

Phase	Sediment characteristics (a)	Depositional process (b)	Landscape and settlement dynamics (c)
(1) Pre-Holocene	• high percentage of gravels (Ø ≥ 2 mm) with clast-supported fabric: base of Del-3, 4, 5 (unit 1)		
(2) Early Holocene	• 1st cycle of fan sediments: Del-3 (units 2, 3)		
(3) Middle Holocene	• 2nd cycle of fan sediments: Del-3 (units 4, 5), Del-4 (unit 2) • 3rd cycle of fan sediments: Del-3 (units 6, 7), Del-4 (units 3, 4), Del-5 (units 2, 3) • Geyikli floodplain + extreme flood events + post-depositional process: Del-2 (units 1, 2, 3, 4, 5)		
(4) Mid- to Late Holocene transition	• soil formation on the Deliktaş alluvial fan and Geyikli floodplain: Del-2 (unit 5), Del-3 (unit 7?), Del-4 (unit 4), Del-5 (unit 3)		
(5) Beginning of the Late Holocene	• 4th cycle of fan sediments: Del-2 (units 6, 7), Del-3 (units 8, 9), Del-4 (unit 5), Del-5 (units 4, 5) • age inversion • sediment extension downwards the distal fan • soils were buried by alluvial fan progradation		
(6) Late Holocene (after 1.5 ka BP)	• 5th cycle of fan sediments: Del-6 (units 2, 3, 4) • sediments younger than 1.5 ka BP rest directly on weathered bedrock (unit 1, Del-6) • sediment hiatus • lateral extension toward the southern hillslope		
(7) Recent 100 years	—		

facilitated lower geomorphodynamics (Dusar et al., 2011), as it is also the case in the Deliktaş catchment (Table 4).

Beginning of Late Holocene (phase 5)

The Mid-Holocene pedofacies on the Deliktaş alluvial fan and Geyikli floodplain were covered—and by this fossilized—by a Late Holocene cycle of coarse- and fine-textured alluvial fan deposits (Del-2, units 6–7; Del-3, units 8–9; Del-5, units 4–5; Figure 4A). Thus, the fan experienced pronounced progradation, growing downslope faster than upslope (phase 5; Table 4). Old sediments stored along the transportation pathways were reworked as evidenced by the age inversion in Del-5, unit 5 (4290–3699 cal yr BP, 77 cm b.s.), a phenomenon widely
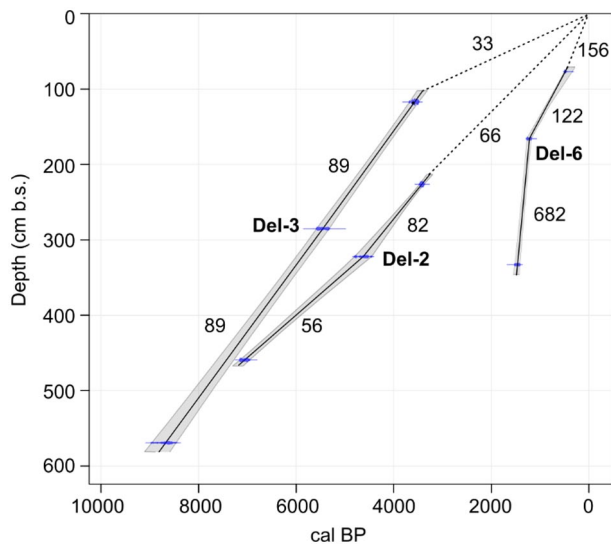
Figure 5. The simplified age-depth modeling of profiles Del-2, Del-3, and Del-6, with the values showing the aggradation rate in cm ka⁻¹ of each section.

discussed for the sediment cascade model in alluvial–colluvial archives (Fryirs, 2013; Fryirs et al., 2007; Lang and Hönscheidt, 1999). Subsuming, for the Deliktaş area, the fifth phase is interpreted as a phase of increased geomorphodynamics coming along with increased erosion and deposition processes (Table 4). Radiocarbon age of 2336–2148 cal yr BP in the middle of this phase (Del-4, unit 5, 85 cm b.s.; Table 3) points to the increase of geomorphodynamics prior to 2.3 cal ka BP. Considering that radiocarbon ages from buried topsoils could represent the maximum age of burial time (Nykamp et al., 2020; Scharpenseel and Schiffmann, 1977), the fifth phase might have predominately continued between ca. 4–3.4 and 2.3 cal ka BP (Table 3) during the beginning of the Late Holocene.

Since this initial Late Holocene phase, the Geyikli floodplain sediments cannot be detected anymore at the sampling locations, prevented by the accumulation of Deliktaş fan and its coinciding spatial growth (Figure 4A; Table 4). The autogenic adjustment of the river channel and floodplain (Croudace and Rothwell, 2015), being reported in the micro-region (Schneider et al., 2015) and western Türkiye (Özpolat et al., 2020), however, cannot be proven in this area.

The intensification of geomorphodynamics, thus, the augmentation of erosion processes in the Deliktaş catchment might be triggered by both human interference and climate change (phase 5; Table 4), as frequently observed in wide areas of the eastern Mediterranean during ca. 5–3 ka BP (Dusar et al., 2011; Kuzucuoğlu et al., 2011; Roberts et al., 2019a, 2019b).

Evidence for settlement activities in the Deliktaş catchment is given by the archeological sites of Zindan Tepe and Hatipler Kalesi (Zimmermann et al., 2015) (Figure 2), which have been used latest since the Bronze to the Iron ages (Supplemental Table S1, available online) (Ludwig et al., 2022). This, together with the ceramic remain found in Del-4, unit 5 (Supplemental Figure S4, available online), suggests human activities that likely affected the soil erosion. This is analogous to multiple studies in the Pergamon micro-region where the Middle to Late Holocene landscape shifted from natural to cultural, including processes of woodland clearing, pasture, and agriculture (Schneider et al., 2017; Shumilovskikh et al., 2016; Yang et al., 2023). Many findings all over the Mediterranean region also emphasize the interrelation between settlement activities and land degradation during the Bronze Age (e.g. Dusar et al., 2011; Jouffroy-Bapicot et al., 2021; Vita-Finzi, 1969, and references therein).

Beyond, rapid climate changes, including the 4.2 and 3.2 ka BP events (Bini et al., 2019; Hazell et al., 2022; Manning et al., 2020; Roberts et al., 2011), under altogether semi-arid conditions (Finné et al., 2019; Wanner et al., 2008) might have amplified torrential run-off (Anderson et al., 2007; Bintliff, 2002) and landscape degradation in the eastern Mediterranean (Dusar et al., 2011). This could have intensified the catchment erosive potential and consequently increased alluvial fan deposition (Butzer, 2005). Such a scarce vegetation cover is documented for the areas around the Deliktaş catchment since ca. 3.5 ka BP (Shumilovskikh et al., 2016, 2022).

In the Mediterranean area, accelerated slope erosion is described at several locations, for example, Arslantepe (eastern Türkiye) (Dreibrodt et al., 2014), albeit few were observed during the time of increased geomorphodynamics in the Deliktaş area (Dusar et al., 2011). This may result from research material bias (Ocakoğlu et al., 2022; Verstraeten et al., 2017) and response time variations among alluvial, fluvial, and lacustrine sediments (Becker et al., 2020; Nykamp et al., 2021; Wanner et al., 2008). Beside the contribution of climate change and human interference, various features in alluvial development and the increase in geomorphodynamics could also be associated with complex natural characteristics (Butzer, 1980; Szabó et al., 2010), for example, initial landform and bedrock/soil type (Butzer, 2005; Fediuk et al., 2019; Szabó et al., 2010), threshold difference in geomorphological locations (or the sediment sources and sinks) (Bakker et al., 2013; Nemec and Kazancı, 1999), and variation in landscape sensitivity to accumulation and erosion (Becker et al., 2020).

Late Holocene (phases 6–7)

Since ca. 1.5 ka BP, sediments were deposited directly on the weathered bedrock at the fan's proximal zone (Del-6, units 2–4; Figure 4A). This sediment hiatus corresponds to a concomitant higher-energetic process evidenced by the highest aggradation rate among the phases (Figure 5), suggesting a new phase of increased geomorphodynamics (phase 6; Table 4). The (sub) rounded shape of pebbles in Del-6, unit 2 (Figure 4A) confirms transport processes by running water and excludes its origin as debris from mass movements at the slopes (cf. Miall, 2006). This further denotes the lateral upslope extension of the alluvial fan (Table 4). These young sediments exposed in Del-6 were roughly deposited contemporaneously to the valley bottom sediments in the nearby Tekkedere catchment (Yang et al., 2023), probably corresponding to the "Younger Fill" (Vita-Finzi, 1969) in the Mediterranean valleys (Roberts, 2014; Roberts et al., 2019b). The time of erosion should take place after the beginning of the Late Holocene (phase 5: ca. 4/3.4–2.3 ka BP; Table 4) and before the onset of deposition at Del-6 (ca. 1.5 ka BP; Table 3), thus, during the profound transformation from the Hellenistic to Roman Imperial period (300 BCE to 300 CE) in the Pergamon micro-region.

In the rural catchment of Deliktaş and its surroundings, the increased number of archeological sites (Supplemental Table S1, available online; Ludwig et al., 2022) corresponds to this micro-regional development. This increased spatial distribution of human settlements indicates the exploitation of formerly untouched lands (Figure 2), likely for arboricultural, pastoral, and agricultural practices (Shumilovskikh et al., 2016, 2022). This presumably caused fundamental changes in the ecosystem and thereby increased the erosive susceptibility of the landscape, leading to intensified gullying in the Deliktaş catchment. During this period, intensified geomorphodynamics are also observed at various locations in the micro-region (Becker et al., 2020), for example, in the rural catchments of the Geyikli river (Schneider et al., 2013, 2014), the Tekkedere creek (Yang et al.,

2023), and in ancient harbor cities and their immediate surroundings (Fediuk et al., 2019; Seeliger et al., 2013, 2019; Shumilovskikh et al., 2016).

In the Deliktaş area, only one cycle of alluvial sediments was observed during the Late Holocene (Figure 4A) and is in chronological order with the boost of archeological sites (Ludwig et al., 2022) (phase 6; Table 4). In contrast, in the nearby Tekkedere catchment, several alluvial cycles were observed for the same period (Yang et al., 2023); the difference may be related to a more continuous settlement of the Tekkedere catchment at multiple locations since the Bronze Age (Ludwig, 2020a; Michalski, 2021), beyond the diversity in land use or landform.

Since the 20th century, the construction of the irrigation system and reservoir remarkably changed the hydrological and geomorphological conditions in the Deliktaş area (phase 7; Table 4). The Geyikli river was straightened to a canal (Doğramacı canal) with embankments (Schneider, 2014). Both the Deliktaş fan and the adjoining Bakırçay plain owe well-developed irrigation systems and abandoned (distributary) channels (Figure 2).

Conclusions

To improve the understanding of the geomorphological history of alluviation, pedogenesis, and erosion, and their driving factors in rural areas of the ancient city of Pergamon, we integrate geomorphological observation in the Deliktaş catchment and the receiving Geyikli river, analyses of alluvial fan and floodplain sediments, and radiocarbon datings. The highly changing sediment texture in the five profiles depicts that the landscape experienced at least seven phases of profoundly different geomorphodynamics. Deliktaş channel sediments deposited in the Late Pleistocene were covered by sediments of an aggrading alluvial fan during the Early–Middle Holocene. Middle Holocene fossil soils on the Deliktaş fan and Geyikli floodplain indicate landscape stability. An accelerated fan growth and hereby a major increase in geomorphodynamics (phase 5) during ca. 4–2 ka BP coincides with the onset of local settlement activities on hitherto untouched lands under the supra-regional aridization with rapid climate changes, possibly including the 4.2 and 3.2 ka BP drought events. Consequences of soil erosion processes on a local scale, that is, the first/second-order catchments, are soil degradation and accelerated growth of fan deposits at their confluence to the foreland, and – on a regional scale – floodplain aggradation such as that of Geyikli and Bakırçay rivers (Becker et al., 2020, 2022b; Schneider et al., 2015).

Pronounced sediment hiatus and lateral extension of fan sediments might indicate increased geomorphodynamics before 1.5 ka. The contemporarily increased number of archeological sites in the Deliktaş area suggests that land use expanded largely to more untouched hillslopes to meet the demand of a growing population in the city of Pergamon and its micro-region, especially during the Roman Imperial period (Laabs and Knitter, 2021). However, uncertain sedimentological and especially chronological results hinder a clear relation between the phases of increased geomorphodynamics in the last 2.5 ka and the major phase of human activities, that is, the transformation of the Pergamon micro-region between the Hellenism and the Roman Imperial Past. On the contrary, our results indicate a more pronounced increase in geomorphodynamic activity since the beginning of the Late Holocene. This phenomenon is also observed in the Tekkedere catchment (Yang et al., 2023) in the vicinity of the Deliktaş catchment, but not generally in all parts of the micro-region (Becker et al., 2020), such as the harbor of Elaia which silted up in the first millenium CE (Seeliger et al., 2013, 2019). Thus, intra-micro-regional variabilities, such as relief, bedrock, and human activities (Yang et al., 2021), are important aspects to understand the geomorphodynamic pattern in a micro-region and wider regions such as the eastern Mediterranean.

ORCID iDs

Xun Yang https://orcid.org/0000-0002-2246-5306
Fabian Becker https://orcid.org/0000-0001-6981-7164
Moritz Nykamp https://orcid.org/0000-0003-2074-1511
Bernhard Ludwig https://orcid.org/0000-0003-0955-9823
Mehmet Doğan https://orcid.org/0000-0002-3815-4203

Supplemental material

Supplemental material for this article is available online.

References

Aksan ZM, Ludwig B, Pirson F, et al. (2022) Ballık Cave. In: Pirson F (ed.) *Pergamon – Die Arbeiten in der Kampagne 2020*. Berlin: Archäologischer Anzeiger, Deutsches Archäologisches Institut/German Archaeological Institute, pp.40–47.

Anderson DG, Maasch KA, Sandweiss DH, et al. (2007) Chapter 1 - Climate and culture change: exploring Holocene transitions. In: Anderson DG, Maasch KA and Sandweiss DH (eds) *Climate Change and Cultural Dynamics*. Cambridge: Academic Press, pp.1–23.

Bakker J, Paulissen E, Kaniewski D, et al. (2013) Climate, people, fire and vegetation: New insights into vegetation dynamics in the Eastern Mediterranean since the 1st century AD. *Climate of the Past* 9: 57–87.

Becker F, Yang X, Doğan M, et al. (2022a) Arbeiten der Physischen Geographie. In: Pirson F (ed.) *Pergamon – Die Arbeiten in der Kampagne 2021*. Berlin: Archäologischer Anzeiger, Deutsches Archäologisches Institut/German Archaeological Institute, pp.62–69.

Becker F, Yang X, Nykamp M, et al. (2022b) Sedimentologische Arbeiten der Physischen Geographie. In: Pirson F (ed.) *Pergamon – Die Arbeiten in der Kampagne 2020*. Berlin: Archäologischer Anzeiger, Deutsches Archäologisches Institut/German Archaeological Institute, pp.50–59.

Becker F, Knitter D, Nykamp M et al. (2020) Meta-analysis of geomorphodynamics in the Western Lower Bakırçay Plain (Aegean Region, Turkey). *Land* 9: 1–29.

Bini M, Zanchetta G, Perşoiu A et al. (2019) The 4.2 ka BP event in the Mediterranean region: An overview. *Climate of the Past* 15: 555–577.

Bintliff J (2002) Time, process and catastrophism in the study of Mediterranean alluvial history: A review. *World Archaeology* 33: 417–435.

Blaauw M (2010) Methods and code for 'classical' age-modelling of radiocarbon sequences. *Quaternary Geochronology* 5: 512–518.

Blair TC and McPherson JG (1994) Alluvial fans and their natural distinction from rivers based on morphology, hydraulic processes, sedimentary processes, and facies assemblages. *Journal of Sedimentary Research* 64: 450–489.

Blair TC and McPherson JG (2009) Processes and forms of alluvial fans. In: Parsons AJ and Abrahams AD (eds) *Geomorphology of Desert Environments*, 2nd edn. Berlin: Springer, pp.413–467.

Brock F, Higham T, Ditchfield P et al. (2010) Current Pretreatment Methods for AMS radiocarbon dating at the Oxford Radiocarbon Accelerator Unit (ORAU). *Radiocarbon* 52: 103–112.

Brown AG (1997) *Alluvial Geoarchaeology: Floodplain Archaeology and Environmental Change*. Cambridge: Cambridge University Press.

Buggle B, Glaser B, Hambach U et al. (2011) An evaluation of geochemical weathering indices in loess–paleosol studies. *Quaternary International* 240: 12–21.

Bull WB (1991) *Geomorphic Responses to Climatic Change*. New York City: Oxford University Press.

Butzer KW (1980) *Holocene Alluvial Sequences: Problems of Dating and Correlation*. In: Cullingford RA, Davidson DA and Lewin J (eds) *Timescales in Geomorphology*. Chichester: John Wiley & Sons, pp.131–142.

Butzer KW (2005) Environmental history in the Mediterranean world: Cross-disciplinary investigation of cause-and-effect for degradation and soil erosion. *Journal of Archaeological Science* 32: 1773–1800.

Collins PEF, Rust DJ, Salih Bayraktutan M, et al. (2005) Fluvial stratigraphy and palaeoenvironments in the Pasinler Basin, eastern Turkey. *Quaternary International* 140–141: 121–134.

Coulthard TJ, Macklin MG and Kirkby MJ (2002) A cellular model of Holocene upland river basin and alluvial fan evolution. *Earth Surface Processes and Landforms* 27: 269–288.

Crema ER and Bevan A (2021) Inference from large sets of radiocarbon dates: Software and methods. *Radiocarbon* 63: 23–39.

Croudace IW and Rothwell RG (2015) *Micro-XRF Studies of Sediment Cores: Applications of a Non-destructive Tool for the Environmental Sciences*. Berlin: Springer.

Danacioğlu Ş and Tağıl Ş (2017) Evaluation of the erosion risk by using the RUSLE model in Bakırçay basin (in Turkish). *Balıkesir Üniversitesi Sosyal Bilimler Enstitüsü Dergisi* 20: 1–18.

Dean WE (1974) Determination of carbonate and organic matter in calcareous sediments and sedimentary rocks by loss on ignition; comparison with other methods. *Journal of Sedimentary Research* 44: 242–248.

Dearing JA (1994) *Environmental Magnetic Susceptibility: Using the Bartington MS2 System*. Kenilworth: Chi Publishing.

Dearing JA, Dann RJL, Hay K et al. (1996) Frequency-dependent susceptibility measurements of environmental materials. *Geophysical Journal International* 124: 228–240.

Di Rita F and Magri D (2009) Holocene drought, deforestation and evergreen vegetation development in the central Mediterranean: A 5500 year record from Lago Alimini Piccolo, Apulia, southeast Italy. *The Holocene* 19: 295–306.

Di Rita F, Michelangeli F, Celant A et al. (2022) Sign-switching ecological changes in the Mediterranean Basin at 4.2 ka BP. *Global and Planetary Change* 208: 1–8.

Doğan T, İlkmen E and Kulak F (2021) A new national 1 MV AMS laboratory at TÜBİTAK MRC in Turkey. *Nuclear Instruments and Methods in Physics Research Section B: Beam Interactions with Materials and Atoms* 509: 48–54.

Dorn RI (1994) The role of climatic change in alluvial fan development. In: Abrahams AD and Parsons AJ (eds) *Geomorphology of Desert Environments*. Dordrecht: Springer Netherlands, pp.593–615.

Dreibrodt S, Lubos C, Lomax J et al. (2014) Holocene landscape dynamics at the tell Arslantepe, Malatya, Turkey – Soil erosion, buried soils and settlement layers, slope and river activity in a middle Euphrates catchment. *The Holocene* 24: 1351–1368.

Dusar B, Verstraeten G, Notebaert B et al. (2011) Holocene environmental change and its impact on sediment dynamics in the Eastern Mediterranean. *Earth-Science Reviews* 108: 137–157.

Eastwood WJ, Leng MJ, Roberts N et al. (2007) Holocene climate change in the eastern Mediterranean region: A comparison of stable isotope and pollen data from Lake Gölhisar, southwest Turkey. *Journal of Quaternary Science* 22: 327–341.

Emre Ö, Özalp S and Dogan A (2005) *Izmir yakın çevresinin diri fayları ve deprem potansiyelleri* (Active faults and earthquake potential in the Izmir region). Ankara: Maden Tetkik ve Arama Genel Müdürlüğü (General Directorate of Mineral Research and Exploration), pp.1–80.

Fediuk A, Wilken D, Wunderlich T et al. (2019) Marine seismic investigation of the ancient Kane harbour bay, Turkey. *Quaternary International* 511: 43–50.

Finné M, Holmgren K, Sundqvist HS et al. (2011) Climate in the eastern Mediterranean, and adjacent regions, during the past 6000 years – A review. *Journal of Archaeological Science* 38: 3153–3173.

Finné M, Woodbridge J, Labuhn I et al. (2019) Holocene hydroclimatic variability in the Mediterranean: A synthetic multiproxy reconstruction. *The Holocene* 29: 847–863.

Florenzano A, Mercuri AM, Rinaldi R et al. (2017) The representativeness of Olea pollen from olive groves and the late Holocene landscape reconstruction in Central Mediterranean. *Frontiers in Earth Science* 5: 1–11.

Fowler AJ, Gillespie R and Hedges REM (1986) Radiocarbon dating of sediments. *Radiocarbon* 28: 441–450.

Fryirs K (2013) (Dis)Connectivity in catchment sediment cascades: A fresh look at the sediment delivery problem. *Earth Surface Processes and Landforms* 38: 30–46.

Fryirs KA, Brierley GJ, Preston NJ et al. (2007) Buffers, barriers and blankets: The (dis)connectivity of catchment-scale sediment cascades. *Catena* 70: 49–67.

Goldberg P and Macphail RI (2006) *Practical and Theoretical Geoarchaeology*. Hoboken, NJ: Blackwell Publishing.

Günther G, Clemen T, Duttmann R et al. (2021) Of animal husbandry and food production—A first step towards a modular agent-based modelling platform for socio-ecological dynamics. *Land* 10: 1–25.

Hazell CJ, Pound MJ and Hocking EP (2022) High-resolution Bronze Age palaeoenvironmental change in the Eastern Mediterranean: exploring the links between climate and societies. *Palynology* 46: 1–20.

Heiri O, Lotter AF and Lemcke G (2001) Loss on ignition as a method for estimating organic and carbonate content in sediments: Reproducibility and comparability of results. *Journal of Paleolimnology* 25: 101–110.

Jouffroy-Bapicot I, Pedrotta T, Debret M et al. (2021) Olive groves around the lake. A ten-thousand-year history of a Cretan landscape (Greece) reveals the dominant role of humans

in making this Mediterranean ecosystem. *Quaternary Science Reviews* 267: 1–24.

Karacik Z, Yilmaz Y and Pearce J (2007) The Dikili-çandarlı volcanics, western Turkey: Magmatic interactions as recorded by petrographic and geochemical features. *Turkish Journal of Earth Sciences* 16: 493–522.

Kassambara A (2023) *ggpubr: 'ggplot2' Based Publication Ready Plots. R Package Version 0.6.0.*

Knitter D, Blum H, Horejs B et al. (2013) Integrated centrality analysis: A diachronic comparison of selected Western Anatolian locations. *Quaternary International* 312: 45–56.

Kuzucuoğlu C, Dörfler W, Kunesch S et al. (2011) Mid- to late-Holocene climate change in central Turkey: The Tecer Lake record. *The Holocene* 21: 173–188.

Laabs J and Knitter D (2021) How much is enough? First steps to a social ecology of the Pergamon microregion. *Land* 10: 1–19.

Lang A and Hönscheidt S (1999) Age and source of colluvial sediments at Vaihingen–Enz, Germany. *Catena* 38: 89–107.

Laufer E (2015) Der neue Survey auf der Kane-Halbinsel (Kane Regional Harbour Survey). In: Pirson F (ed.) *Pergamon – Bericht über die Arbeiten der Kampagne 2014*. Berlin: Archäologischer Anzeiger, Deutsches Archäologisches Institut/German Archaeological Institute, pp.139–150.

Ludwig B (2020a) Das Umland von Pergamon. Die Arbeiten des Umland-Surveys 2019. In: Pirson F (ed.) *Pergamon – Das neue Forschungsprogramm und die Arbeiten in der Kampagne 2019*. Berlin: Archäologischer Anzeiger, Deutsches Archäologisches Institut/German Archaeological Institute, pp.205–216.

Ludwig B (2020b) Reconstructing the ancient route network in Pergamon's surroundings. *Land* 9: 1–39.

Ludwig B (2023) *Beyond the City of Pergamon. A Landscape Archaeological Study of the Pergamon Micro-Region From the Hellenistic to the Roman Imperial Period*. Berlin: Department of Earth Sciences, Freie Universität Berlin, 1–269.

Ludwig B, Pirson F, Aksan ZM, et al. (2022) Das Umland von Pergamon. Die Arbeiten des Umland-surveys 2021. In: Pirson F (ed.) *Pergamon – Die Arbeiten in der Kampagne 2021*. Berlin: Archäologischer Anzeiger, Deutsches Archäologisches Institut/German Archaeological Institute, pp.48–62.

Manning SW, Lorentzen B, Welton L et al. (2020) Beyond megadrought and collapse in the Northern Levant: The chronology of Tell Tayinat and two historical inflection episodes, around 4.2ka BP, and following 3.2ka BP. *PLoS ONE* 15: 1–38.

McHugh C, Seeber L, Cormier M et al. (2006) Submarine earthquake geology along the North Anatolia Fault in the Marmara Sea, Turkey: A model for transform basin sedimentation. *Earth and Planetary Science Letters* 248: 661–684.

Miall A (2014) *Fluvial Depositional Systems*. Cham: Springer International Publishing.

Miall AD (2006) *The Geology of Fluvial Deposits: Sedimentary Facies, Basin Analysis, and Petroleum Geology*. Berlin: Springer.

Michalski P (2021) *A Rural Settlement in the Surroundings of Pergamon - Survey Analysis of the Kuyulu Kaya in the Lower Western Kaikos Valley*. Berlin: Humboldt-Universität zu Berlin, pp.1–292.

Moscariello A (2018) Alluvial fans and fluvial fans at the margins of continental sedimentary basins: Geomorphic and sedimentological distinction for geo-energy exploration and development. *Geological Society London Special Publications* 440: 215–243.

Nalbant SS, Hubert A and King GCP (1998) Stress coupling between earthquakes in northwest Turkey and the north Aegean Sea. *Journal of Geophysical Research Solid Earth* 103: 24469–24486.

Nemec W and Kazancı N (1999) Quaternary colluvium in west-central Anatolia: Sedimentary facies and palaeoclimatic significance. *Sedimentology* 46: 139–170.

Niwa Y, Sugai T, Saegusa Y et al. (2011) Use of electrical conductivity to analyze depositional environments: Example of a Holocene delta sequence on the Nobi Plain, central Japan. *Quaternary International* 230: 78–86.

Nykamp M, Becker F, Braun R et al. (2021) Sediment cascades and the entangled relationship between human impact and natural dynamics at the pre-pottery Neolithic site of Göbekli Tepe, Anatolia. *Earth Surface Processes and Landforms* 46: 430–442.

Nykamp M, Knitter D and Schütt B (2020) Late holocene geomorphodynamics in the vicinity of Göbekli Tepe, SE Turkey. *Catena* 195: 1–14.

Ocakoğlu F, Kuzucuoğlu C, Akbulut A et al. (2022) Lake level changes and paleo-precipitation estimations based on colluvial stratigraphy of holocene sediments in West Anatolia (Simav Graben). *Palaeogeography Palaeoclimatology Palaeoecology* 597: 1–21.

Özpolat E, Yıldırım C and Görüm T (2020) The Quaternary landforms of the Büyük Menderes Graben system: The southern Menderes Massif, western Anatolia, Turkey. *Journal of Maps* 16: 405–419.

Özpolat E, Yıldırım C, Görüm T et al. (2022) Three-dimensional control of alluvial fans by rock uplift in an extensional regime: Aydın Range, Aegean extensional province. *Scientific Reports* 12: 1–14.

Paradisopoulou PM, Papadimitriou EE, Karakostas VG et al. (2010) Seismic Hazard Evaluation in western Turkey as revealed by stress transfer and time-dependent probability calculations. *Pure and Applied Geophysics* 167: 1013–1048.

Parker G (1999) Progress in the modeling of alluvial fans. *Journal of Hydraulic Research* 37: 805–825.

Peel MC, Finlayson BL and McMahon TA (2007) Updated world map of the Köppen-Geiger climate classification. *Hydrology and Earth System Sciences* 11: 1633–1644.

Pirson F (2017) Die Siedlungsgeschichte Pergamons. Überblick und kritische revision. Mit einem Appendix von Anneke Keweloh-Kaletta. *Istanbuler Mitteilungen* 67: 43–130.

Pirson F (2020) Pergamon – Das neue Forschungsprogramm und die Arbeiten in der kampagne 2019. *Archaologischer Anzeiger* 2: 1–245.

R Core Team (2022) *R: A Language and Environment for Statistical Computing*. Vienna: R Foundation for Statistical Computing.

Reimer PJ, Austin WEN, Bard E et al. (2020) The IntCal20 Northern Hemisphere radiocarbon age calibration curve (0–55 cal kBP). *Radiocarbon* 62: 725–757.

Roberts CN, Woodbridge J, Palmisano A et al. (2019a) Mediterranean landscape change during the Holocene: Synthesis, comparison and regional trends in population, land cover and climate. *The Holocene* 29: 923–937.

Roberts N (2014) *The Holocene: an environmental history*. New York, NY: Wiley Blackwell.

Roberts N, Allcock SL, Barnett H et al. (2019b) Cause-and-effect in Mediterranean erosion: The role of humans and climate upon Holocene sediment flux into a central Anatolian lake catchment. *Geomorphology* 331: 36–48.

Roberts N, Brayshaw D, Kuzucuoğlu C et al. (2011) The Mid-Holocene climatic transition in the Mediterranean: Causes and consequences. *The Holocene* 21: 3–13.

Santisteban JI, Mediavilla R, López-Pamo E et al. (2004) Loss on ignition: A qualitative or quantitative method for organic matter and carbonate mineral content in sediments? *Journal of Paleolimnology* 32: 287–299.

Scharpenseel HW and Schiffmann H (1977) Soil radiocarbon analysis and soil dating. *Geophysical Surveys* 3: 143–156.

Schneider S (2014) *Geoarchaeological Case Studies in the Bakırçay Valley – Paleogeography and Human-Environmental Interactions in the Chora of Pergamon in Western Turkey*. Berlin: Freie Universität Berlin.

Schneider S, Matthaei A, Bebermeier W et al. (2014) Late Holocene human–environmental interactions in the Eastern Mediterranean: Settlement history and paleogeography of an ancient Aegean hill-top settlement. *Quaternary International* 324: 84–98.

Schneider S, Matthaei A, Schlöffel M et al. (2015) A geoarchaeological case study in the chora of Pergamon, western Turkey, to reconstruct the Late Holocene landscape development and settlement history. *Quaternary International* 367: 62–76.

Schneider S, Nykamp M, Matthaei A et al. (2013) Alluvial geoarchaeology of a small drainage basin in western Anatolia: Late Holocene landscape development and the question of the mouth of the Paleo-Bakırçay. *Quaternary International* 312: 84–95.

Schneider S, Schlöffel M, Schwall C et al. (2017) First stratigraphic evidence and absolute dating of a Bronze Age settlement in the Bakırçay valley in western Turkey. *Journal of Archaeological Science Reports* 12: 316–322.

Seeliger M, Bartz M, Erkul E et al. (2013) Taken from the sea, reclaimed by the sea: The fate of the closed harbour of Elaia, the maritime satellite city of Pergamum (Turkey). *Quaternary International* 312: 70–83.

Seeliger M, Pint A, Feuser S et al. (2019) Elaia, Pergamon's maritime satellite: The rise and fall of an ancient harbour city shaped by shoreline migration. *Journal of Quaternary Science* 34: 228–244.

Seeliger M, Pint A, Frenzel P et al. (2017) Foraminifera as markers of Holocene sea-level fluctuations and water depths of ancient harbours — A case study from the Bay of Elaia (W Turkey). *Palaeogeography Palaeoclimatology Palaeoecology* 482: 17–29.

Shumilovskikh L, Seeliger M and Brückner H (2022) Vegetation changes and human impact during the last 3500 years in western Anatolia – A pilot study from the Crater Lake Kara Göl. In: Pirson F (ed.) *Pergamon – Die Arbeiten in der Kampagne 2020*. Berlin: Archäologischer Anzeiger, Deutsches Archäologisches Institut/German Archaeological Institute, pp.72–81.

Shumilovskikh LS, Seeliger M, Feuser S et al. (2016) The harbour of Elaia: A palynological archive for human environmental interactions during the last 7500 years. *Quaternary Science Reviews* 149: 167–187.

Soil Science Division Staff (2017) *Soil Survey Manual*. Washington, DC: United States Department of Agriculture Handbook, p.18.

Szabó J, Dávid L and Lóczy D (2010) *Anthropogenic Geomorphology: A Guide to Man-Made Landforms*. Berlin: Springer.

Terefe T, Mariscal-Sancho I, Peregrina F et al. (2008) Influence of heating on various properties of six Mediterranean soils. A laboratory study. *Geoderma* 143: 273–280.

Ülgen UB, Franz SO, Biltekin D et al. (2012) Climatic and environmental evolution of Lake Iznik (NW Turkey) over the last ~4700 years. *Quaternary International* 274: 88–101.

Van Dijk M, Kleinhans MG, Postma G, et al. (2012) Contrasting morphodynamics in alluvial fans and fan deltas: Effect of the downstream boundary. *Sedimentology* 59: 2125–2145.

Verstraeten G, Broothaerts N, Van Loo M et al. (2017) Variability in fluvial geomorphic response to anthropogenic disturbance. *Geomorphology* 294: 20–39.

Vita-Finzi C (1969) *The Mediterranean Valleys: Geological Changes in Historical Times*. Cambridge: Cambridge University Press.

Walsh K, Berger J-F, Roberts CN et al. (2019) Holocene demographic fluctuations, climate and erosion in the Mediterranean: A meta data-analysis. *The Holocene* 29: 864–885.

Wanner H, Beer J, Bütikofer J et al. (2008) Mid- to Late Holocene climate change: An overview. *Quaternary Science Reviews* 27: 1791–1828.

Weiss H (2016) Global megadrought, societal collapse and resilience at 4.2-3.9 ka BP across the Mediterranean and west Asia. *Past Global Change Magazine* 24: 62–63.

Wei T and Simko V (2021) R package 'corrplot': Visualization of a Correlation Matrix (Version 0.92). Available at: https://github.com/taiyun/corrplot

Wulf U (1994) Der Stadtplan von Pergamon: Zu Entwicklung und Stadtstruktur von der Neugründung unter Philetairos bis in spätantike Zeit. *Istanbuler Mitteilungen* 44: 135–175.

Yang X, Becker F, Knitter D et al. (2021) An overview of the geomorphological characteristics of the Pergamon micro-region (Bakırçay and Madra River catchments, Aegean region, West Turkey). *Land* 10: 1–27.

Yang X, Becker F, Nykamp M, et al. (2022) Dataset of sediment analyses (pH, electrical conductivity, magnetic susceptibility, loss on ignition, and X-ray fluorescence) from the Tekkedere catchment in the Pergamon Micro-Region, western Turkey. In: Yang X (ed). Pangaea.

Yang X, Becker F, Nykamp M et al. (2023) Mid- to late Holocene geomorphodynamics in a long-term settled mountain catchment in the Pergamon micro-region, western Turkey. *Quaternary Research* 114: 69–92.

Yang X, Becker F, Nykamp M, et al. (2023) Dataset of sediment analyses (pH, electrical conductivity, magnetic susceptibility, loss on ignition, and X-ray fluorescence) from the Deliktaş catchment in the Pergamon Micro-Region, western Turkey. In: Yang X (ed). Pangaea.

Zimmermann M (2011) *Pergamon. Geschichte, Kultur, Archäologie*. München: C.H. Beck.

Zimmermann M, Matthaei A and Ateş G (2015) Die Chora von Pergamon: Forschungen Im Kaikostal und in der Antiken Stadt Atarneus. In: Matthaei A and Zimmermann M (eds) *Urbane Strukturen und bürgerliche Identität im Hellenismus*. Heidelberg: Verlag Antike, pp.193–236.